Precise and absolute measurements of the complex third-order optical susceptibility

Stéphane Santran, Lionel Canioni, Laurent Sarger, Thierry Cardinal, Evelyne Fargin

Precise and absolute measurements of the complex third-order optical susceptibility

Stéphane Santran, Lionel Canioni, and Laurent Sarger

Centre de Physique Moléculaire Optique et Hertzienne, Talence Cedex, France

Thierry Cardinal and Evelyne Fargin

Institut de Chimie et de la Matière Condensée de Bordeaux, Talence Cedex, France

We present precise and absolute measurements of full complex third-order optical susceptibility on different fused-silica and original glasses composed of tellurium, titanium, and niobium erbium. These materials are designed to be the key point for applications ranging from high-power laser systems to optoelectronics; their nonlinear index of refraction is a major property and thus must be accurately known. A large dispersion (more than 30%) of the nonlinear index of fused-silica glasses was found. Measurements on tellurium glasses have shown strong nonlinearities, to be linked to the configurations of their cations and anions.

OCIS codes: 120.0120, 120.3180, 190.0190, 190.4400.

1. INTRODUCTION

Many materials have been characterized for real-world applications such as optoelectronic applications, information technology, or solid-state lasers. As one of the most important properties of these materials is their nonlinear index of refraction, it must be accurately known.

In high-power laser systems, optical components are exposed to a high light flux. These materials, such as fused silica, amplifier glasses, or nonlinear crystals, must be chosen to have a small nonlinear index. Nevertheless, the power of the beams used is so strong that optical nonlinearities can alter their propagation. Therefore it is essential to measure the nonlinearity of these materials with high accuracy in order to control these modifications. In the case of the Megajoule Laser (Commissariat a l'Energie Atomique–Centre d'Etudes Scientifiques et Techniques l'Aquitaine), an error of 10% on the nonlinear index can lead to an equivalent error for the beam energy on the target.

Numerous techniques for precise and sensitive measurements of third-order nonlinearities have been proposed in the past decade. Besides the Z-scan techniques,[1,2] spectral analysis,[3] third-harmonic generation,[4,5] and time-resolved interferometry,[6] we have recently demonstrated a new kind of collinear transient absorption experiment,[7] in which the full complex third-order nonlinear susceptibility can be measured.

2. COLLINEAR PUMP–PROBE EXPERIMENT

The aim of this paper is to design a practical setup able to measure absolute and accurate values of the third-order optical susceptibility of materials, mainly for optical glasses. Usually, pump–probe experiments are performed, and a small angle between the pump and the probe for technical ease and for the beam polarization can be arbitrarily chosen. As we have to provide absolute measurements, this experiment used collinear beams, which have the advantage of exact interaction zone knowledge but the disadvantage with respect to polarization choice. First, the experimental setup will be described, and then we will emphasize theoretical and technical approaches needed to extract from the experimental data good and accurate measurements of the nonlinear index. The theoretical point of view will focus on the pulse propagation problem, and the experimental signal and the original acquisition mode for real-time measurement mode will be presented. Finally, the comparison of this technique with the most common Z scan will be discussed.

A. Experimental Setup

The experimental setup (Fig. 1) is organized around an ultralow noise, mode-locked laser source (a Titan sapphire oscillator, eventually frequency doubled) or an optical parametric oscillator providing ultrashort laser pulses (~100 fs). The laser output beam is balanced unevenly in a *p*-polarized pump and in a *s*-polarized probe by use of a half-wave plate and a polarizing cube beam splitter. These two beams are further mixed with another polarizing cube, precisely adjusted to be exactly collinear, and are focused into the sample. The collinearity of the two beams in the sample allows us to perfectly control the interaction zone, which is important for absolute measurement.

Eventually, the pump beam is ejected by the last cube polarizer, and the intensity of the probe beam is recorded as a function of the delay between the two beams (Fig. 4). As the polarizing cubes are not ideal, there are two leakages of the pump beam through the first and the second polarizing cube beam splitters. The leakage of the pump through the first cube (Pol 1 of Fig. 1) goes through the probe arm with a *p* polarization, so this pulse is not at-

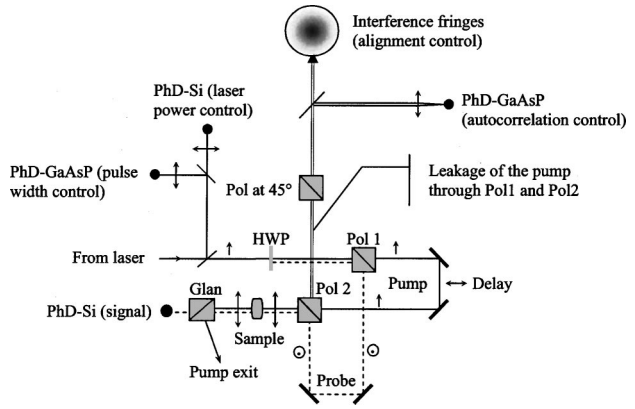

Fig. 1. Experimental setup for measurements of the third-order nonlinear susceptibility at 800 nm. HWP, half-wave plate; Pol, polarizer; PhD-Si, silicon photodiode detector; PhD-GaAsP, gallium arsenic phosphor photodiode detector used as a two-photon photodiode; Glan, Glan polarizer.

tenuated through the second polarizing cube. Because the polarizing cubes are identical, the leakage of the pump beam through the second cube is equivalent to the probe arm's leakage. These two leakages, having the same polarization and the same power, eventually interfere with a high contrast. This can be used as a powerful tool for perfect alignment and as a monitor for pulse duration in this interferometric geometry. Indeed, just by adding a lens and a GaAsP photodiode (two-photon photodiode),[8] one can easily record a second-order autocorrelation.

Further in the experience, a silicon photodiode (one photon) and a GaAsP photodiode (two photons) are used for laser diagnostics. The Si photodiode allows us to monitor the average power, and the GaAsP photodiode allows us to monitor the spatial and temporal pulse parameters (discussed in Subsection 2.D).

B. Complete Theoretical Analysis and Calculus of the n_2

In the particular case of the collinear pump–probe experiment, the transverse aspect of the field can be introduced in a rigorous way. As the pump and probe beams are completely overlapping, the propagation equation suggests a perturbative analysis with transverse variables.

In the temporal space, assuming that the polarization in a point depends only on the electric field in the same point, the general expression of the third-order nonlinear polarization can be written as

$$\begin{aligned}\mathbf{P}_{\mathrm{NL}}^{(3)}(\mathbf{r},\,t) &= \epsilon_0 \int_{-\infty}^{+\infty}\int_{-\infty}^{+\infty}\int_{-\infty}^{+\infty} \overline{\overline{\mathbf{R}^{(3)}}}(t_1,\,t_2,\,t_3) \\ &\quad\times \mathbf{E}(\mathbf{r},\,t-t_3)\mathbf{E}(\mathbf{r},\,t-t_3-t_2) \\ &\quad\times \mathbf{E}(\mathbf{r},\,t-t_3-t_2-t_1)\mathrm{d}t_1\mathrm{d}t_2\mathrm{d}t_3, \quad (1)\end{aligned}$$

where $\overline{\overline{\mathbf{R}^{(3)}}}(t_1,\,t_2,\,t_3)$ is the local response function of the media.

In materials out of resonance, and with the classical Born–Oppenheimer approximation, the effect of the field on materials can be separated into two phenomena with different response times. Under these conditions, the nonlinear polarization is given by Hellwarth[9]:

$$\begin{aligned}\mathbf{P}_{\mathrm{NL}}^{(3)}(\mathbf{r},\,t) &= \epsilon_0 \overline{\overline{\chi^{(3)}}}\mathbf{E}(\mathbf{r},\,t)\mathbf{E}(\mathbf{r},\,t)\mathbf{E}(\mathbf{r},\,t) \\ &\quad+ \epsilon_0 \mathbf{E}(\mathbf{r},\,t)\int_0^{+\infty} \overline{\overline{d^{(3)}}}(t-t_1) \\ &\quad\times \mathbf{E}(\mathbf{r},\,t_1)\mathbf{E}(\mathbf{r},\,t_1)\mathrm{d}t_1. \quad (2)\end{aligned}$$

The first term is the third-order nonlinear electronic polarization of the media. The associated physical process is the electronic cloud bending, which is indeed an ultrafast effect (less than 1 fs). The second one is the third-order nonlinear nuclear polarization. The associated physical effect is the molecules' vibrations and rotations. As this phenomena have a response time longer than that of electronic one (from 100 fs to several nanoseconds), the second term includes a convolution with the material nonlinear complex tensor $\overline{\overline{d^{(3)}}}$. In the collinear pump–probe experiment, as the pump pulse and the probe pulse have perpendicular polarization, the nonlinear polarization can be further developed along the probe axis as

$$\begin{aligned}P_1^{(3)}(r,\,z,\,t) &= 3\epsilon_0\chi_{1212}^{(3)}E_1(r,\,z,\,t)E_2^2(r,\,z,\,t) \\ &\quad+ \epsilon_0 E_1(r,\,z,\,t)\int_0^{+\infty} d_{1122}^{(3)}(t-t_1) \\ &\quad\times E_2^2(r,\,z,\,t_1)\mathrm{d}t_1 \\ &\quad+ 2\epsilon_0 E_2(r,\,z,\,t)\int_0^{+\infty} d_{1212}^{(3)}(t-t_1) \\ &\quad\times E_1(r,\,z,\,t_1)E_2(r,\,z,\,t_1)\mathrm{d}t_1. \quad (3)\end{aligned}$$

The basic equation is obtained from the general propagation equation within the reasonable framework of the dispersionless approximation and without self-steepening. The general equation for the probe beam propagation with nonlinear third-order coupling to the pump beam in isotropic media can be written as

$$\begin{aligned}&\Delta_\perp A_s(r,\,z,\,t) - 2ik(\omega_0)\frac{\partial A_s(r,\,z,\,t)}{\partial z} \\ &\quad= \sigma_1 A_s(r,\,z)|A_p(r,\,z)|^2 + \sigma_2\overline{A_s(r,\,z)}A_p^2(r,\,z), \quad (4)\end{aligned}$$

where $A_s(r,\,z,\,t)$ is the complex amplitude of the probe electric field, $A_p(r,\,z,\,t)$ is the complex amplitude of the pump electric field, z is the spatial variable along the beams' propagation, $r = \sqrt{x^2+y^2}$, and the two expressions σ_1 and σ_2 are equal to

$$\begin{aligned}\sigma_1 &= -\frac{3k_0^2}{2}\chi_{1212}^{(3)}s(t)s^2(t-u) - \frac{k_0^2}{2}s(t) \\ &\quad\times \int_0^{+\infty} d_{1122}^{(3)}(t-t_1)s^2(t-t_1)\mathrm{d}t_1 - \frac{k_0^2}{4}s(t-u) \\ &\quad\times \int_0^{+\infty} d_{1212}^{(3)}(t-t_1)s(t-t_1)s(t-t_1-u)\mathrm{d}t_1, \\ &\quad (5)\end{aligned}$$

$$\sigma_2 = -\frac{k_0^2}{4}\exp(-i2\omega_0 u)\Bigg[3\chi^{(3)}_{1212}s(t)s^2(t-u) + s(t-u)\int_0^{+\infty} d^{(3)}_{1212}(t-t_1)s(t-t_1) \times s(t-t_1-u)\mathrm{d}t_1\Bigg], \quad (6)$$

where $s(t)$ is the temporal shape of the pump or probe pulse and u is the variable delay between the pump and the probe pulses.

As we are dealing with a rather thin sample (1 mm) and short laser pulses of the order of 100 fs, temporal effects on propagation have been shown to be not significant in numerical simulations, and thus they have been neglected in this analysis. Moreover, as we want to keep this experiment as linear as possible, we use moderate pump peak power so that the nonlinear propagation of the pump beam can be neglected.

Although the differential propagation equation cannot be analytically solved, the transient absorption configuration suggests an easier perturbation treatment with respect to the transverse variables of the field. However, the presence in the right-hand side of the complex amplitude and complex conjugate of the probe field complicates, at first glance, the analysis and requires the use of two perturbation variables, σ_1 as the coefficient of $A_s(r, z)$ and σ_2 as the coefficient of $\overline{A_s(r, z)}$. It is worth noting that the perturbation coefficients σ_1 and σ_2 are time dependent. In fact, the differential equation concerns only the transverse aspect of the probe field, and not the time, so the time dependence of the fields can be conveniently included in the perturbation coefficients.

The solution at zero order is taken as the usual fundamental transverse Gaussian mode:

$$A_0(r, z) = \frac{A_0}{w(z)}\exp\left[-\frac{r^2}{w^2(z)}\right] \times \exp\left[-ik(\omega_0)\frac{r^2}{2R(z)}\right]\exp[i\theta(z)]. \quad (7)$$

Then the solution for the probe beam with this perturbative approach restricted to the first order is

$$A_s = A_0 + \sigma_1 A_1 + \bar{\sigma}_1 A_2 + \sigma_2 A_3 + \bar{\sigma}_2 A_4. \quad (8)$$

The substitution of the amplitude A_s in the equation does simplify the development as the solutions A_1 and A_3 are identical and the solutions A_2 and A_4 are equal to the zero-order solution:

$$A_s = A_0 + (\sigma_1 + \sigma_2)A_1. \quad (9)$$

In first order the calculus of the amplitude of the electric field is reduced to the resolution of the differential equation (6), which can be resolved analytically in Fourier space:

$$\Delta_\perp A_1(r, z, t) - 2ik(\omega_0)\frac{\partial A_1(r, z, t)}{\partial z} = A_p(r, z, t)\overline{A_p(r, z, t)}A_0(r, z, t). \quad (10)$$

Finally, the signal due to the probe intensity can be written as

$$I_s \propto I_s^0\left[1 - \frac{k_0^2}{4\sqrt{2}}\frac{P_m T}{c\epsilon_0}F(w_0, k_0, L)Y(u)\right], \quad (11)$$

where P_m is the average power, T is the repetition rate of the laser, and $F(w_0, k_0, L) = \arctan[L/(k_0 n_0 w_0^2)]$ is a numerical factor depending on the spatial properties of the laser beam. In this expression, all the material information arise from the correlation function between the pump and the probe pulses:

$$Y(u) = G(u)[2\beta + \sqrt{\alpha^2+\beta^2}\sin(2\omega_0 u - \phi)] + [H^2(\Re(d^{(3)}_{1212}), u) + H^2(\Im(d^{(3)}_{1212}), u)]^{1/2} \times \sin(2\omega_0 u - \psi) - H(\Im(d^{(3)}_{1212}), u) - H(\Im(d^{(3)}_{1122}), u), \quad (12)$$

with the following definitions:

α and β are the real and imaginary parts of the electronic third-order optical susceptibility, respectively: $\alpha = \Re(\chi^{(3)}_{1111})$, $\beta = \Im\chi^{(3)}_{1111}$ with the classical property for the third-order nonlinear susceptibility; $\chi^{(3)}_{1111} = 3\chi^{(3)}_{1212}$ for a isotropic medium;

$$G(u) = \frac{\int_{-\infty}^{+\infty} s(t)s(t-u)\mathrm{d}t}{\left[\int_{-\infty}^{+\infty} s(t)\mathrm{d}t\right]^2}$$

is the correlation function for the electronic contribution of the signal;

$$H(f, u) = \frac{\int_{-\infty}^{+\infty}\left[s(t)s(t-u)\int_0^{+\infty} f(t-t_1)s(t-t_1)s(t-t_1-u)\mathrm{d}t_1\right]\mathrm{d}t}{\left[\int_{-\infty}^{+\infty} s(t)\mathrm{d}t\right]^2}$$

is the correlation function for the nuclear contribution; $\phi = \arctan(-\beta/\alpha)$ is the phase of the electronic nonlinear fringes; and $\psi = \arctan[\Im(d^{(3)}_{1212})/\Re(d^{(3)}_{1212})]$ is the phase of the nuclear nonlinear fringes.

Expression (11) shows that the useful signal corresponds to the probe intensity variations within the coherence zone, arising from either electronic or nuclear coupling contributions. These two types of variation are proportional to the average power of the pump beam and to the repetition rate of the laser and depend on the main characteristics of the laser (wavelength and beam waist) and of the sample to analyze (linear index and sample length). These variations are representative of the coupling between the pump pulse and the probe pulse in the sample via the nondiagonal electronic and nuclear complex tensor elements. The signal shape is driven by the function $Y(u)$, where u is the delay between the pump and the probe pulses. The two origins are different and deserve detailed analysis.

First, in the (main) electronic contribution, two terms in Eq. (12) will control the probe beam intensity: a zero frequency term proportional to the imaginary part of the $\chi^{(3)}$ (β is always positive), which represents the nonlinear absorption, and an oscillating term—at twice the optical frequency versus delay (the nonlinear fringes)—proportional to the modulus of $\chi^{(3)}$.

Second, for the nuclear contribution, three terms in Eq. (12) will then control the probe intensity: one oscillating term—also at twice the optical frequency versus the delay—depending on the real and imaginary parts of $d^{(3)}_{1212}$ and two zero frequency terms proportional to the imaginary parts of $d^{(3)}_{1212}$ and $d^{(3)}_{1122}$. Whatever the sign of the imaginary parts of $d^{(3)}_{1212}$ or $d^{(3)}_{1122}$, Raman gain or loss can be expected.

$G(u)$ is a temporal term, delay dependent. At zero delay, this function is equal to the ratio between the second-order momentum of $s(t)$ and the squared first-order momentum of $s(t)$. It represents how the intensity of the light is spread along the pulse. For example, this function is equal (for the same temporal width τ_0 fs) to $1/(\tau_0\sqrt{2\pi}) = 0.3989/\tau_0$ for a Gaussian pulse, $1/(3\tau_0) = 0.3333/\tau_0$ for a secant hyperbolic pulse, and $1/\tau_0$ for a rectangular one.

$H(f, u)$ is a more complicated term owing to the noninstantaneous response time of the Raman phenomena. So this function includes the correlation of a classical convolution of the material response function with the temporal shape of the laser pulse.

More obvious, $F(w_0, k_0, L)$ is a spatial term, which includes the beam waist w_0, the linear index of refraction n_0, and the sample thickness L.

Both approaches can then be done, to perform either relative or absolute measurements of the nonlinear indices.

For the simplest case of relative measurements, if the temporal characterization and the average power of the laser are not required, the beam waist and the wavelength of the laser must be accurately known owing to dependence of the function $F(w_0, k_0, L)$ on the thickness and the linear index. On the other hand, for absolute measurements, all the characteristics of the laser must be known accurately and especially the temporal profile of the pulse $s(t)$.

This analytical analysis of the propagation equation has been obtained with the following approximations: dispersion, self-steepening of the probe beam, and nonlinear propagation of the pump beam that is neglected. The leading parameter for validation of these approximations is indeed the self-phase modulation length of the pump (the propagation length corresponding to a $\pi/4$ nonlinear phase shift): $L_{\mathrm{SPM}} = \pi w_0^2/2k_0 n_2 P_c$. This length must be larger than the thickness of the sample. With an average power of 500 mW and a waist of 30 μm, this length can be as long as 17.3 cm in the fused silica but as small as a few millimeters in a strong nonlinear glass (tellurium glasses).

C. Effect of the Nuclear Contribution to the Signal (Theoretical Aspect)

This collinear pump–probe experiment is not too sensitive to nuclear phenomena. If the signal measured by this experiment includes the nuclear contribution, nevertheless, its signature will be also included in the electronic contribution in the so-called nonlinear fringes. As an example, Fig. 2 presents a simulated signal for liquid CS_2. We intentionally display the three different fringe envelopes contributing to the signal. Previous measurements of the CS_2 nonlinearity with a Mach–Zehnder interferometer[11] by use of the same pulsed laser (100 fs) have shown two nuclear contributions. In this case, the electronic nonlinearity accounts for 19% of the total nonlinear signal, whereas a fast nuclear nonlinearity, with a measured response time of 170 fs, is the main contribution (64%). Finally, a smaller nuclear orientation nonlinearity, with a measured response time τ_r of 880 fs, accounts for 17%. The imaginary part of the nuclear nonlinearity was undetected, even within our high experimental accuracy. With these results, the collinear pump–probe signal can be computed and presented in Fig. 2. First, the electronic signal (solid thin curve) shows a nonlinear absorption appearing as a dissymmetry between the top and the bottom of the signal envelope.

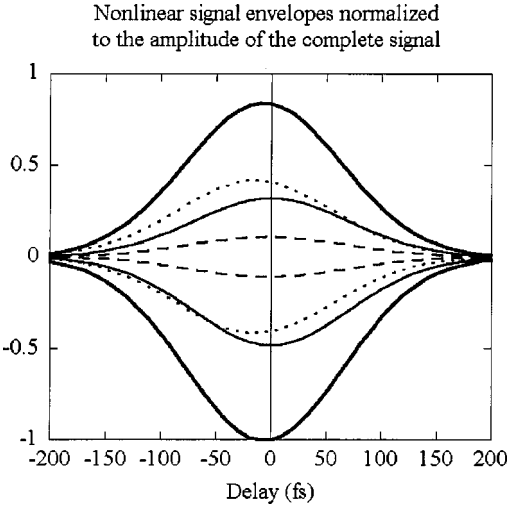

Fig. 2. Theoretical signal with a 1-mm sample of CS_2. This signal is calculated at 800 nm for a 100-fs-width laser pulse. There are three contributions to the signal: the electronic one (solid thin curve), the nuclear orientation one (long-dashed curve), and the fast nuclear one (short-dashed curve). The solid curve is the full envelope signal. The curves have been computed with the tensor element definitions studied by Owyoung[10]: $d_{1122}(t) = -A\exp(-t/\tau_r)$, $d_{1221}(t) = d_{1212}(t) = (3A/2)\exp(-t/\tau_r)$, and $d_{1111}(t) = 2A\exp(-t/\tau_r)$, where A is the amplitude of the nuclear phenomena and τ_r is the response time of this process.

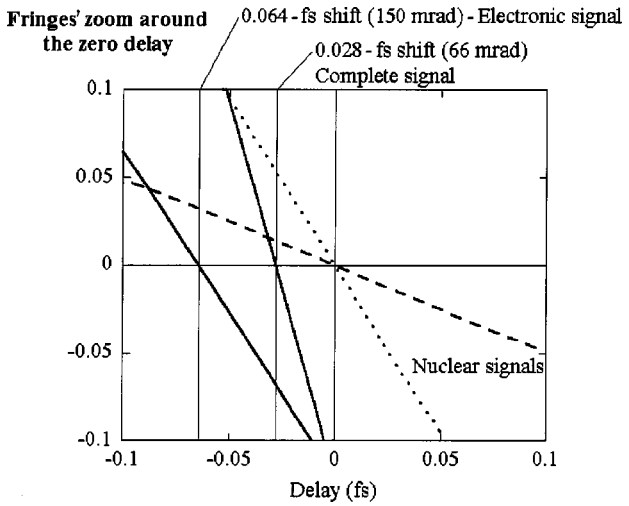

Fig. 3. Zoom of the nonlinear fringes around the zero delay for the CS_2 signal. There are three contributions to the signal: the electronic one (solid thin curve), the nuclear orientation one (long-dashed curve), and the fast nuclear one (short-dashed curve). These phase shifts of the nonlinear fringes have been computed for intelligibility but are not experimentally detectable.

The fast nuclear nonlinear signal (short dashed curve) is shifted approximately tens of femtoseconds. Owing to the relative long response time (880 fs), the reorientation signal (long dashed curve) is not significantly shifted. Figure 3 shows a zoom of the nonlinear fringes for all these nonlinear contributions around zero delay ($u = 0$ fs). This figure shows indeed a very small phase shift of the electronic nonlinear fringes (150 mrad, corresponding to a delay of 0.064 fs) due to the nonlinear absorption present in the term: $\phi = \arctan(-\beta/\alpha)$. In contrast, there is no phase shift in the nuclear signals. The nonlinear absorption in the CS_2 induces a phase shift on the full signal of approximately 66 mrad (0.028 fs).

All these results are theoretical calculations using results on the CS_2 to explain the theoretical analysis exposed previously. Nevertheless, this eventual small shift of the envelope of the signal or the possible phase of the nonlinear fringes can be either difficult (signal comparison with the autocorrelation) or even impossible to measure in any experiment as, in fact, the moving delay between the pump and the probe cannot be precise enough to determine the zero-delay position.

Practically, only the amplitude of the nonlinear fringes around the zero-delay position and the amplitude shift in the presence of nonlinear absorption can be measured and analyzed.

D. Experimental Signal

The signal in Fig. 4 displays the photoelectric signal of the probe beam (in volts) versus the delay between the pump and the probe (in femtoseconds) for a silicon sample (wafer, 1 mm thick). The main characteristics are a mean value reflecting the nonlinear absorption and an oscillating behavior that accounts for the expected coupling between the pump and the probe in the sample through the nondiagonal $\chi^{(3)}$ tensor elements. This signal is experimentally superimposed on the unavoidable linear mixing between the probe and a leak of the pump acting as a noise. A straightforward Fourier analysis of the experimental signal is displayed in Fig. 5. It clearly isolates the linear mixing (linear fringes classically oscillating at the optical frequency) and the nonlinear coupling (nonlinear fringes).[7] By this technique, the measurement of the amplitude of the nonlinear fringes and the nonlinear absorption allows us to characterize the $\chi^{(3)}$ tensor elements of isotropic materials.

Two modes of acquisition are then possible: either use of a lock-in amplifier coupled to an oscilloscope that requires a slow-moving delay (note the frequency of the fringes in Fig. 5) so as to give time for the lock-in amplifier to average the signal or, in a more effective way, use of a fast multichannel personal computer acquisition card (sampling frequency of 250 kHz). A rapid scan of the delay at a 10-Hz rate will lead to a quasi-real-time experiment. Also, in the first acquisition mode, a Fourier transform can be performed to measure the nonlinear effect. Technically, the Fourier transform is applied to only 512 points on a signal of more than 9000 points around the zero delay where the nonlinear signal is at its maximum. In this small window the nonlinear fringes can be compared with a simple sinusoid without amplitude variation, and a flat-top filter—a short-pulse response filter—directly in the Fourier space [Eq. (13)] will lead to the correct amplitude:

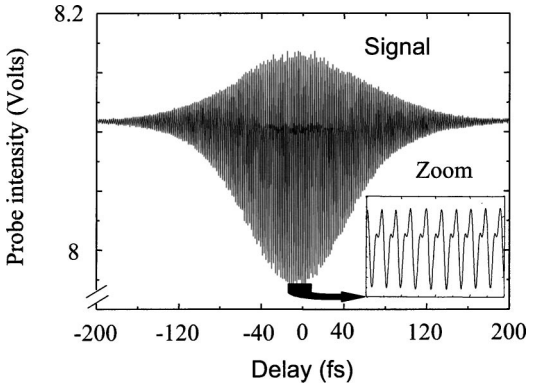

Fig. 4. Experimental signal obtained from a sample of silicon at 1.5 μm. This signal was acquired at low-speed delay.

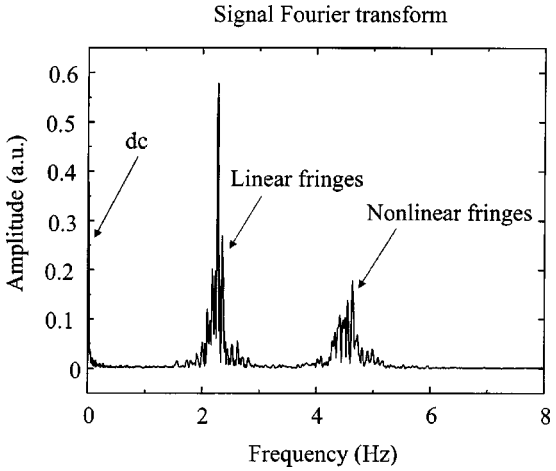

Fig. 5. Fourier transform of the signal obtained on the silicon sample (Fig. 4).

Table 1. Synthesis of Error Studies in this Paper[a]

Parameters	Relative Accuracy (%)	Absolute Accuracy (%)
Average power	—	5%–7%
Wavelength	<0.1%	<0.1%
Repetition rate	—	<0.1%
Beam waist	2%–3% (800 and 1500 nm) 3%–4% (400 nm)	2%–3% (800 and 1500 nm) 3%–4% (400 nm)
Temporal width	—	3%–5% (800 and 1500 nm) 4%–10% (400 nm)
Nonlinear amplitude fringes	0.1%–10%	0.1%–10%
Sample thickness	0.1%–1%	0.1%–1%
Sample linear index	0.1%–2%	0.1%–2%
Full accuracy	2%–16% (800 and 1500 nm) 3%–17% (400 nm)	10%–28% (800 and 1500 nm) 12%–34% (400 nm)

[a] The table shows the relative and absolute accuracy ranges that strongly depend on the sample optical quality and on the laser wavelength.

$$\sum_{k=-\mu}^{\mu} a_k \delta(f-k), \qquad a_k = a_{-k}, \qquad \begin{matrix} \mu = 4, & a_1 = -0.934516, & a_3 = -0.179644 \\ a_0 = 1, & a_2 = 0.597986, & a_4 = 0.015458 \end{matrix}. \tag{13}$$

The final analysis consists of measuring the height of the dc and the nonlinear peaks to calculate the real and imaginary parts of the third-order optical susceptibility. As beam parameters such as the average power and the time width are acquired simultaneously with one- and two-photon photodiodes[8] (previously calibrated with a power meter and an autocorrelation), the calculated values are not affected by eventual deviations of the laser. We have recently demonstrated (not published) that the two-photon absorption in the photodiode and the nonlinear signal in the sample result from the same third-order nonlinear effect. So, these two signals have the same deviations when the pulse width or the beam waist of the laser changes. Consequently, the sample nonlinear signal's eventual deviations can be corrected with the two-photon photodiode signal in real time.

All this analysis is thus performed in quasi real time and allows powerful signal optimization. We found it pertinent to adjust the position of the sample in the waist precisely, and we were even able to detect eventual parasitic signals due to coupling into the laser cavity. This experimental protocol has been proven reliable, and we make use of the high repetition rate of the laser oscillator and delay scan rate to average the measured data and increase furthermore the signal-to-noise ratio.

The accuracy of the nonlinear measurement (including all the nonlinear effects: nuclear and electronic) will greatly depend on the laser parameters. A standard, straightforward—although tedious—procedure can tie the experimental parameters' accuracy on average power, beam size, and temporal shape to the absolute error margin. Table 1 presents our efforts to reach a (record) value of 10%. Nevertheless, the relative error bars, owing to an excellent signal-to-noise ratio, is routinely well below 2% even for weakly nonlinear samples.

For comparison purposes, we deduce the usual nonlinear index from the above results by using the classical formulation (in SI); conversion to the electrostatic unit (esu) system is also presented:

$$n_2(\mathrm{m^2/W}) = \frac{3\chi^{(3)}_{1111}(\mathrm{m^2/V^2})}{2c\epsilon_0 n_0^2}, \tag{14}$$

$$n_2(\mathrm{m^2/W}) = \frac{80\pi}{n_0 c} n_2 \ (\mathrm{esu}). \tag{15}$$

E. Comparison with the Z-Scan Technique

This collinear pump–probe technique can be roughly compared with the single-beam Z-scan technique by one's substituting the scan of the sample around the waist by the delay between the pump and the probe. Nevertheless, the time resolution greatly improves the data analysis. Obviously, the Z-scan experiment appears easier to implement but is proven sensitive to eventual scattering and phase distortion due to the sample. The usual measurement must be performed on good optical quality samples. In the present experiment, as the signal is due to the coherent nonlinear coupling between the pump and the probe, it is less affected by static phase defaults, and measurements of low nonlinearity samples in the early stage of development have been carried out.

3. EXPERIMENTAL RESULTS

In the following results on fused-silica and some oxide glasses, no gain or nonlinear absorption (β coefficient) or imaginary parts of the nuclear nonlinear coefficients, the equation describing the probe intensity variations can be simplified as

$$I_s \propto I_s^0 \left[1 - \frac{k_0^2}{4\sqrt{2}} \frac{P_m T}{c\epsilon_0} F(w_0, k_0, L) Y(u) \right], \tag{16}$$

with

$$Y(u) = [\alpha G(u) + H(\Re(d^{(3)}_{1212}), u)] \sin(2\omega_0 u). \tag{17}$$

Moreover, in the fused-silica or oxide glasses, the amplitude of the nuclear phenomena is too weak to be evaluated in this experimental setup. So, electronic and nuclear phenomena are measured as a whole and are collected in one single parameter. Finally, the probe intensity variations can be written for the following measurements as

$$I_s \propto I_s^0 \left[1 - \frac{k_0^2}{4\sqrt{2}} \frac{P_m T}{c\epsilon_0} F(w_0, k_0, L) \Lambda G(u) \sin(2\omega_0 u) \right]. \tag{18}$$

Λ is the global nonlinear third-order nonlinear susceptibility, including electronic and nuclear nonlinear phenomena.

A. Nonlinearities in Fused Silica

Fused silica is the material of choice for fabrication of lenses and windows for high-power lasers owing to its exceptionally large transparency windows and industrial optical quality. We will nevertheless point out the unexpected large variation of the nonlinearity of different samples of fused silica from different fabrication processes. Our measurements at several wavelengths will be compared with available experimental values, and the observed dispersion will be analyzed by use of two theoretical models: the Kramers–Kronig dispersion law[12] and the pertubative model.[13] Finally, noninstantaneous nonlinearities for these samples will be emphasized with Raman spectra.

1. Nonlinear Index Measurement

There are essentially two types of fused silica: natural fused silica and pure synthetic fused silica. Table 2 displays our results obtained at 800 and 400 nm. Synthetic samples present a smaller value than natural ones but a difference larger than 30% is clearly demonstrated, although the linear index will be affected only by less than 1%.

Variations of the nonlinear index of refraction at 800 nm have also been observed at 400 nm, which confirm these differences.

Table 2. Absolute Measurements of the Nonlinear Index of Refraction of Several Samples of Fused Silica[a]

Sample of Fused Silica	Nonlinear index at 800 nm (10^{-16} cm^2/W)	Nonlinear index at 400 nm (10^{-16} cm^2/W)
Heraeus S300	3.5	4.0
Herasil	3.3	3.3
Suprasil	3.2	3.4
Heraeus Homosil	3.1	3.4
Heraeus S1	3.0	3.4
Herasil S1V	3.0	3.4
Suprasil EN1027A	2.7	3.3
F851053	2.7	3.0
Heraeus H1	2.6	3.3
Schott SQ1	2.5	2.8

[a] Relative accuracy between the different samples is inferior to 1%.

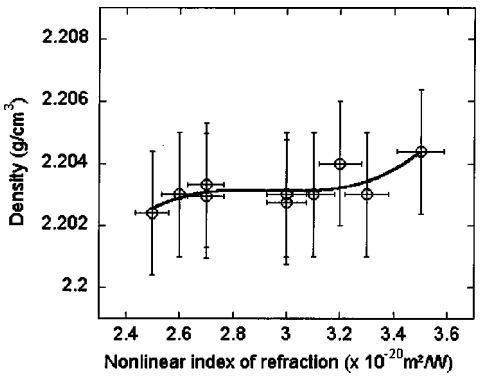

Fig. 6. Density of fused-silica samples as a function of the nonlinear index of refraction. The solid curve is a fit.

Few clues can be pointed out to account for this rather large and surprising deviation. Although some empirical relations have linked the nonlinearity (electronic) to the bandgap,[14] they will not be applied here; all the samples tested here have similar bandgaps in the 200-nm region and are excited in the near infrared. Although no correlation has been found, clearly a trend between residual absorption (due to impurities) and nonlinearity can be seen in our experimental data. Another way will be to explore a link between density and nonlinearity more likely to happen. Obviously, the material density is proportional to the small entities' (SiO_2) concentration. As the macroscopic polarization is globally the product of the microscopic contribution times the number of the active entities, one expects that density and the nonlinear index of refraction would be strongly coupled. Figure 6, indeed, shows such a trend, but a more accurate density measurement is necessary to confirm this argument.

Nonlinear index mapping has been made on several samples. Some of them present small inhomogeneities that can induce some variations on the measurement of the same sample if the position of the beam has moved. It is worth noting that these commercial samples present an overall homogeneity much higher than that of experimental samples. This greatly eases the measurement procedure.

The influence of density (and fluctuation) of the material as well as the amount of residual impurity will be further analyzed to eventually enhance the performance of the industrial process with respect to the nonlinearity.

2. Dispersion of the Nonlinear Index

Using the same technique, we measure the nonlinear index of one standard fused-silica sample—Suprasil—at three wavelengths: 400, 800, and 1500 nm.

The values are 3.4×10^{-20} m^2/W at 400 nm, 3.2×10^{-20} m^2/W at 800 nm, and 2.5×10^{-20} m^2/W at 1500 nm.

The relationship among the nonlinear index n_2, the linear index, and its dispersion as first proposed by the Boling–Glass–Owyoung theory[15] has been long accepted, and many transparent materials have successfully been screened.[16] As this theory predicts only the low-frequency behavior of the nonlinearity, no differential dispersion can be found between linear and nonlinear indices. This model has been widely improved with another

approach[17] taking into account mainly two-photon absorption. Those authors used a two-band model to calculate the nonlinear absorption. The corresponding nonlinear refractive index is simply retrieved with the Kramers–Kronig transformation [Eq. (19)]. They were able to predict an especially good scaling in a wealth of different materials, ranging from semiconductors to insulators, and even proposed an universal dispersion curve. More recently a new perturbation theory analysis[13] [PERT equation (20)] has been proposed for the dispersion of the nonlinear refractive index. We also take into account other published nonlinear measurements for analysis by use of these two powerful models:

$$n_2(\text{esu}) = K' \frac{\sqrt{E_p}}{n_0 E_g^4} G_2(\hbar\omega/E_g), \tag{19}$$

with

$$G_2(x) = \frac{1}{2x^6}\left[-\frac{3}{8}x^2(1-x)^{-1/2} + 3x(1-x)^{1/2} - 2(1-x)^{3/2} + 2\theta(1-2x)(1-2x)^{3/2}\right],$$

where $E_p = 2|p_{vc}|^2/m_0$, p_{vc} is the interband momentum matrix element, m_0 is the free-electron mass, E_g is the gap energy, and K' is a constant that takes different values according to the material, and

$$\frac{n_2(x)}{n_2(0)} = \frac{n(0)}{n(x)}\left[\frac{n(x)^2+2}{n(0)^2+2}\right]^4 \frac{1}{1-x^2}\left[\frac{1-x^2}{1-4x^2} + \frac{1}{2K} \times \left(\frac{1-x^2}{1-4x^2} - \frac{1+x^2/3}{1-x^2}\right)\right] \tag{20}$$

(x is in inverse centimeters and K is the kurtosis electron distribution,[15] which has a value close to 0.5 for wide-bandgap glasses).

This analysis is summarized in Fig. 7. The quality of our absolute measurement and accuracy allows us to review the usual conclusion and find that the observed discrepancies are rather more affected by the sample origin than by the measurement technique.

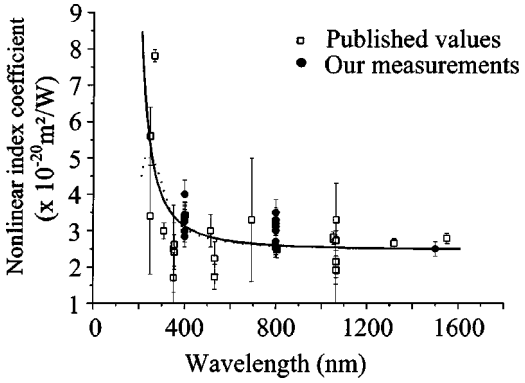

Fig. 7. Measured values of the nonlinear refractive-index coefficient as a function of wavelength. Coefficients are plotted in multiples of $1 \times 10^{-20}\,\text{m}^2/\text{W}$. The source of the data is indicated in Ref. 18. The solid curve is a fit of the data by the PERT equation, and the dashed curve is a fit of the Kramers–Kronig model.

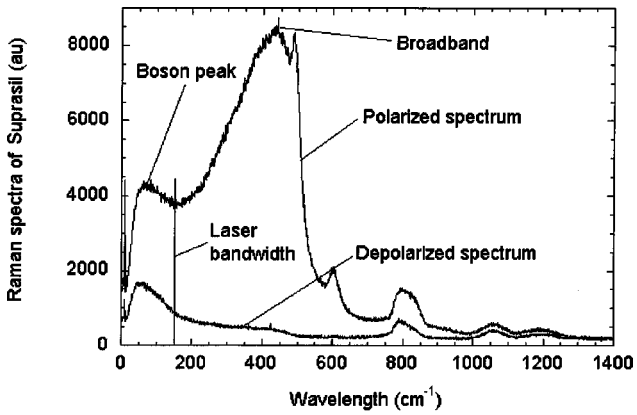

Fig. 8. Polarized and depolarized low-frequency Raman spectra of a sample of fused silica (Suprasil), excited at 514.5 nm.

3. Nonresonant Vibrational Contributions

Our experimental approach for nonlinearity measurements relies on femtosecond laser pulses, whereas nanosecond pulses are usually used in high-power laser chains. If electronic contributions in glasses are identical for femtosecond and nanosecond pulse excitations, nuclear contributions are not identical. The corresponding noninstantaneous nonlinearity will strongly depend on the spectral width of the excited pulses and then indirectly on the temporal width of these pulses. To study the influence of the nonresonant vibrational contribution, we compute the noninstantaneous signal with experimental polarized and depolarized Raman spectra displayed in Fig. 8.

Two dominant low-frequency components are clearly visible in the Raman spectra of SiO_2 (quasi similar for all the samples of fused silica) in the Raman spectra: a broadband at 450 cm^{-1} attributed to the out-of-plane rocking of the oxygen in the bridging Si—O—Si and a Boson peak[19] associated with acousticlike excitations. For a 100-fs laser pulse, the frequency components are excited up to 150 cm^{-1}, corresponding to the Boson peak.

By using the response function symmetry properties of the nuclear contribution and following the model proposed by Hellwarth[9] and Stolen and Tomlinson,[20] one can extract first the nuclear nonlinear susceptibility and then the two independent real nonlinear response functions $d^{(3)}_{1122}(t)$ and $d^{(3)}_{1212}(t)$ from Raman spectra corrected by the Boltzman factor: $[1 - \exp(-\hbar\omega/kT)]^{-1}$. These response functions are presented in Fig. 9. It is worth noting that Eq. (12) shows that in the case of no Raman loss or gain—which is the case in a bulk of fused silica—the nuclear nonlinear polarization depends only on the response function $d^{(3)}_{1212}(t)$.

As suggested by Stolen and Tomlinson,[20] we compute the Raman contribution to the nonlinear effective index of fused silica for pulses of different widths (Fig. 10). The nonlinear Raman contribution begins to be significant for pulses longer than 100 fs and reaches the maximum for a pulse width of 10 ps. In contrast to Stolen and Tomlinson's findings, negative Raman contribution to n_2 due to a quadratic phase has not been found for extremely

short pulses in our case. The reason is that the transient absorption technique does not give the sign of the nonlinear index but only the modulus. Nevertheless, this negative contribution measured in fibers disappears for pulses longer than 30 fs. As our experimental conditions are the use of pulses longer than 100 fs and the measure of a thin fused-silica bulk, the nuclear contribution cannot be negative. Figure 10 shows that, in our experience, the nuclear contribution to the signal cannot be more than 5%. As Hellwarth *et al.*[21] has found that approximately 18% of the nonlinear index of refraction in fused silica is attributed to the Raman effect, we can conclude that a maximum Raman contribution is approximately 1% in our signal. The more recent measurements of Smolorz and Wise[22] (who measured a nuclear fraction between 13% and 18% in SiO_2—GeO_2 fibers) confirm this conclusion.

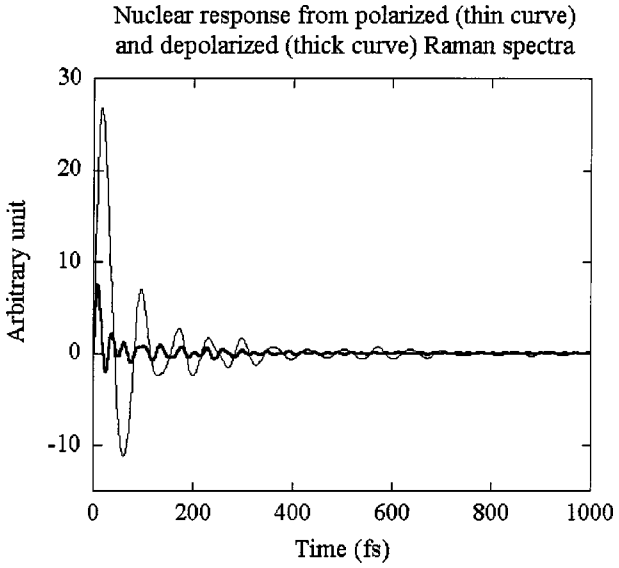

Fig. 9. Nuclear response functions $d_{1122}(t)$ (thin curve) and $d_{1212}(t)$ (thick curve) of fused-silica glass, calculated from the Raman spectra shown in Fig. 5.

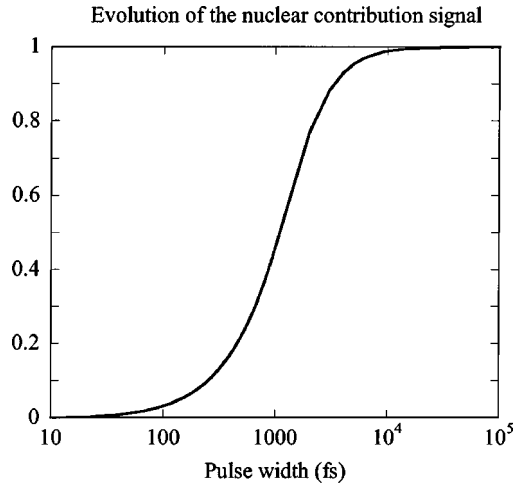

Fig. 10. Calculated evolution of the nuclear contributions arising from the response $d_{1212}(t)$ of the nonlinear signal in arbitrary units as a function of the temporal width.

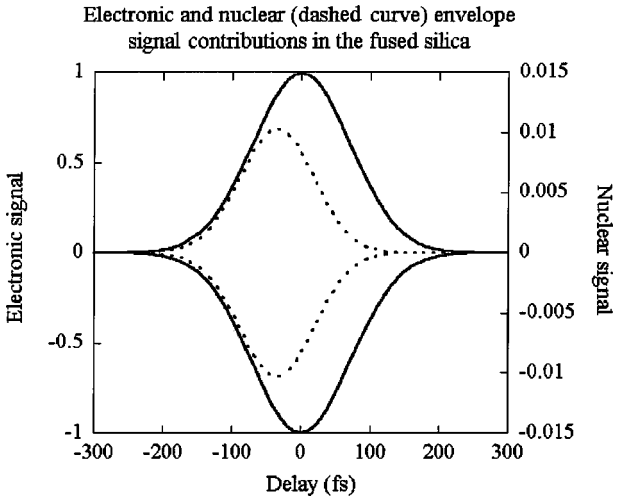

Fig. 11. Pure theoretical signal of a 1-mm sample of fused silica at 800 nm with a 100-fs-width laser pulse. Nuclear contribution to the signal represents 1.5%.

In consideration of this result, the nuclear signal has been computed and compared with the electronic one on Fig. 11. As the decrease of the response function $d^{(3)}_{1212} \times (t)$ is relatively short, the envelope of the nuclear signal is shifted several tens of femtoseconds. This temporal shift is similar to the shift of the CS_2 fast nuclear nonlinear signal on Fig. 2. Nevertheless, in consideration of the error bars of our measurements, the Raman contribution can easily be neglected in these analyses, and we can conclude that pure electronic nonlinear susceptibility measurements are possible in fused silica.

B. Nonlinearities in Oxide Glasses

1. High Nonlinearity and Material Science

The development of new glassy materials for photonic devices or all-optical communication systems requires glass composition choices that are dictated by the necessity of increasing the nonlinear optical efficiency.[23,24] A comparative study[25] on oxide glasses identifies some promising compositions (gallate and tellurite glasses) in terms of nonlinear index and figures of merit. In this context the identification of the microscopic origin of the optical nonlinearities in glasses proves to be essential. Among the candidates inducing the largest nonlinear indices when introduced into oxide glasses, heavy cations with ns^2 electron pairs (Te^{4+}, Tl^{+}, Pb^{2+}...) or d^0 ions (Ti^{4+}, Nb^{5+}...) can be studied. The relationship between structural properties of such oxide glasses and optical (nonlinear) properties has already been largely discussed first theoretically in Lines[26] and then experimentally intensively.[27–30] An optimization of nonlinear efficiencies was consecutively performed, leading to a gain of 1 or 2 orders of magnitude when compared with fused-silicate glasses. Here we will review the nonlinear performances for different oxide glass matrices that contain increasing proportions of additive niobium oxide. Third-order nonlinear measurements are precisely correlated to structural data.

Concerning the noninstantaneous contribution to the nonlinearity of these high nonlinear glasses, the Raman contribution in these glasses can be four times higher

than in fused silica.[31] Nevertheless, that means that the Raman contribution to our signal cannot exceed 4%, which is in the error bars of these sample measurements—their optical quality is less good than in the commercial fused-silica samples. So we can conclude that our measurements are quite pure electronic ones for the tellurium and niobium glasses.

2. Measurements and Origin of the Nonlinearity in Niobium Glasses

Niobium oxide[32] has been introduced in borate, either sodium or calcium borophosphate glass matrices (Fig. 12).

The nonlinearity of a calcium borophosphate glass with the largest concentration of niobium can reach values around 25 times the fused-silica response. Indeed, these d^0 niobium transition metals form oxygenated sites $(Nb—O)_6$ in oxide glasses in which oxygen electrons are delocalized toward niobium atoms to form metal–oxygen bonds. This phenomenon gives rise to large hyperpolarizabilities of $(Nb—O)_6$ entities. The nonlinear response is then currently proportional to the niobium concentration for $(Nb—O)_6$ isolated oxygenated sites in the poorest niobium glasses regardless of the glass matrix.

An enhancement of the nonlinear response is observed for the richest niobium borophosphate glasses. This has been explained by the progressive formation of two-dimensional and then three-dimensional associations of niobium-oxygenated sites. The creation of Nb—O—Nb bridges increases the delocalization of $(Nb—O)_6$ electronic clouds, inducing an enhancement of each $(Nb—O)_6$ site hyperpolarizability.

The nonlinear absorption of these materials remains very small, around ten times the silica glass's nonlinear absorption level. Indeed, the contribution to the imaginary part of the third-order nonlinear susceptibility is essentially due to a two-photon absorption process. The differences between presented glass compositions are not significant for their absorption edge slightly evolving from 300 to 380 nm; thus no correlation can be established between the absorption-edge position and the nonlinear absorption.

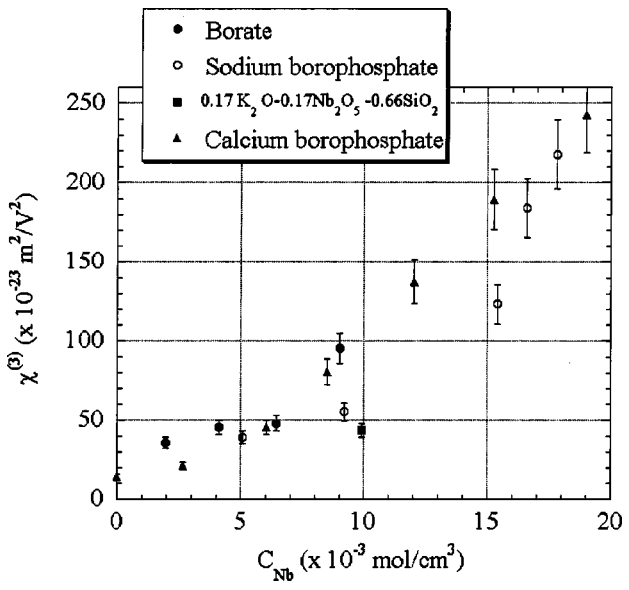

Fig. 12. Measurement of the real part of the third-order optical susceptibility of glasses as a function of the concentration in niobium at 800 nm.

4. CONCLUSION

Transient absorption experiments show a high efficiency on the measurement of nonlinearities in isotropic materials. The sensitivity of the experiment has been exploited to study either weak or strong nonlinearities. The accuracy of this technique allows precise measurement of various fused silica as well as to finely optimize oxide glasses for optronic applications.

Fundamentally, we now investigate the surface nonlinearities with an equivalent setup. Although, in our conditions, the surface does not contribute to the measurement of the nonlinear index within the volume as the number of hyperpolarizable entities is small, it will be interesting to study the nonlinear properties of glasses and crystals at the surface. For example, it has been already shown[33] that $\chi^{(3)}_{\text{surface}}$ is higher than $\chi^{(3)}_{\text{volume}}$ at the air–dielectric interface by use of third-harmonic generation.

ACKNOWLEDGMENTS

We acknowledge the financial support of the Atomic Energy Commission and the University of Bordeaux I. We thank M. Couzi for the low-frequency Raman spectra of fused silica and appreciate the technical assistance of Philippe Lemaire and Claude Lalaude.

S. Santran, the corresponding author, can be reached by e-mail at stephane.santran@laposte.net.

REFERENCES

1. M. Sheik-Bahae, A. A. Said, and E. W. Van Stryland, "High-sensitivity, single-beam n_2 measurements," Opt. Lett. **14**, 955–957 (1989).
2. M. Sheik-Bahae, A. A. Said, T. Wei, D. J. Hagan, and E. W. Van Stryland, "Sensitive measurement of optical nonlinearities using a single beam," IEEE J. Quantum Electron. **26**, 760–769 (1990).
3. E. T. J. Nibbering, M. A. Franco, B. S. Prade, G. Grillon, C. Le Blanc, and A. Mysyrowicz, "Measurement of the nonlinear refractive index of transparent materials by spectral analysis after nonlinear propagation," Opt. Commun. **119**, 479–484 (1995).
4. D. J. Moss, H. M. van Driel, and J. E. Sipe, "Third harmonic generation as a structural diagnostic of ion-implanted amorphous and crystalline silicon," Appl. Phys. Lett. **48**, 1150–1152 (1986).
5. J. E. Sipe, D. J. Moss, and H. M. van Driel, "Phenomenological theory of optical second- and third-harmonic generation from cubic centrosymmetric crystals," Phys. Rev. B **35**, 1129–1141 (1987).
6. K. Minoshima, M. Taiji, and T. Kobayashi, "Femtosecond time-resolved interferometry for the determination of complex nonlinear susceptibility," Opt. Lett. **16**, 1683–1685 (1991).
7. M. O. Martin, L. Canioni, and L. Sarger, "Measurements of complex third-order optical susceptibility in a collinear pump–probe experiment," Opt. Lett. **23**, 1874–1876 (1998).
8. J. K. Ranka, A. L. Gaeta, A. Baltuska, M. S. Pshenichnikov, and D. A. Wiersma, "Autocorrelation measurement of 6-fs pulses based on the two-photon-induced photocurrent in a GaAsP photodiode," Opt. Lett. **22**, 1344–1346 (1997).

9. R. W. Hellwarth, *Third-Order Susceptibilities of Liquids and Solids*, Part I of Vol. 5 of Monographs: Progress in Quantum Electronics, J. H. Sanders and S. Stenholm, eds. (Pergamon, New York, 1977).
10. A. Owyoung, "The origins of the nonlinear refractive indices of liquids and glasses," Ph.D. dissertation (California Institute of Technology, Pasadena, Calif., 1971).
11. L. Canioni, "Liquids and glasses nonlinearities properties analyzed by femtosecond interferometry," Ph.D. thesis (University of Bordeaux, Bordeaux, France, 1994).
12. M. Sheik-Bahae, D. C. Hutchings, D. J. Hagan, and E. W. Van Stryland, "Dispersion of bound electron nonlinear refraction in solids," IEEE J. Quantum Electron. **27**, 1296–1309 (1991).
13. R. Adair, L. L. Chase, and S. A. Payne, "Dispersion of the nonlinear refractive index of optical crystals," Opt. Mater. (Amsterdam, Neth.) **1**, 185–194 (1992).
14. A. A. Said, M. Sheik-Bahae, D. J. Hagan, T. H. Wei, J. Wang, J. Young, and E. W. Van Stryland, "Determination of bound-electronic and free-carrier nonlinearities in ZnSe, GaAs, CdTe, and ZnTe," J. Opt. Soc. Am. B **9**, 405–414 (1992).
15. N. L. Boling, A. J. Glass, and A. Owyoung, "Empirical relationships for predicting nonlinear refractive index changes in optical solids," IEEE J. Quantum Electron. **14**, 601–608 (1978).
16. I. Kang, T. Krauss, F. Wise, B. G. Aitken, and N. F. Borrelli, "Femtosecond measurement of enhanced optical nonlinearities of sulfide glasses and heavy-metal-doped oxide glasses," J. Opt. Soc. Am. B **12**, 2053–2059 (1995).
17. M. Sheik-Bahae, D. J. Hagan, and E. W. Van Stryland, "Dispersion and band-gap scaling of the electronic Kerr effect in solids associated with two-photon absorption," Phys. Rev. Lett. **65**, 96–99 (1990).
18. D. Milan, "Review and assessment of measured values of the nonlinear refractive-index coefficient of fused silica," Appl. Opt. **37**, 546–550 (1998).
19. C. McIntosh, J. Toulouse, and P. Tick, "The Boson peak in alkali silicate glasses," J. Non-Cryst. Solids **222**, 335–341 (1997).
20. R. H. Stolen and W. J. Tomlinson, "Effect of the Raman part of the nonlinear refractive index on the propagation of ultrashort optical pulses in fibers," J. Opt. Soc. Am. B **9**, 565–573 (1992).
21. R. W. Hellwarth, J. Cherlow, and T. T. Tang, "Origin and frequency dependence of nonlinear optical susceptibilities of glasses," Phys. Rev. B **11**, 964–967 (1975).
22. S. Smolorz and F. Wise, "Measurement of the nonlinear optical response of optical fiber materials by use of spectrally resolved two-beam coupling," Opt. Lett. **24**, 1103–1105 (1999).
23. G. Lenz, J. Zimmermann, T. Katsufuji, M. E. Lines, H. Y. Hwang, S. Spälter, R. E. Slusher, S.-W. Cheong, J. S. Sanghera, and I. D. Aggarwal, "Large Kerr effect in bulk Se-based chalcogenide glasses," Opt. Lett. **25**, 254–256 (2000).
24. J. M. Harbold, F. O. Ilday, F. W. Wise, and B. G. Aitken, "Highly nonlinear Ge—As—Se and Ge—As—S—Se glasses for all-optical switching," IEEE Photonics Technol. Lett. **14**, 822–824 (2002).
25. M. E. Lines, "Oxide glasses for fast photonic switching: a comparative study," J. Appl. Phys. **69**, 6876–6884 (1991).
26. M. E. Lines, "Bond-orbital theory of linear and nonlinear electronic response in ionic crystals. II. Nonlinear response," Phys. Rev. B **41**, 3383–3390 (1990).
27. A. Berthereau, E. Fargin, A. Villesuzanne, R. Olazcuaga, G. Le Flem, and A. Ducasse, "Determination of local geometries around tellurium in TeO_2—Nb_2O_5 and TeO_2—Al_2O_3 oxide glasses by XANES and EXAFS: investigation of electronic properties of evidenced oxygen clusters by *ab initio* calculations," J. Solid State Chem. **126**, 143–151 (1996).
28. S. Le Boiteux, P. Segonds, L. Canioni, L. Sarger, T. Cardinal, C. Duchesne, E. Fargin, and G. Le Flem, "Nonlinear optical properties for TiO_2 containing phosphate, borophosphate, and silicate glasses," J. Appl. Phys. **81**, 1481–1487 (1997).
29. E. Fargin, A. Berthereau, T. Cardinal, J. J. Videau, A. Villesuzanne, and G. Le Flem, "Contribution of theoretical chemistry to the investigation of optical non linearities in glasses," Ann. Chim. Sci. Mater. **23**, 27–32 (1998).
30. B. Jeansannetas, S. Blanchandin, P. Thomas, P. Marchet, J. C. Champarnaud-Mesjard, T. Merle-Méjean, B. Frit, V. Nazabal, E. Fargin, and G. Le Flem, "Glass structure and optical nonlinearities in thallium (I) Tellurium (IV) oxide glasses," J. Solid State Chem. **146**, 329–335 (1999).
31. S. Montant, "Second and third order nonlinear studies in glasses," Ph.D. thesis (University of Bordeaux, Bordeaux, France, 1999).
32. T. Cardinal, E. Fargin, G. Le Flem, and S. Le Boiteux, "Correlations between structural properties of Nb_2O_5—$NaPO_3$—$Na_2B_4O_7$ glasses and nonlinear optical activities," J. Non-Cryst. Solids **222**, 228–234 (1997).
33. T. Y. F. Tsang, "Optical third-harmonic generation at interfaces," Phys. Rev. A **52**, 4116–4125 (1995).